Hindawi
Advances in Condensed Matter Physics
Volume 2022, Article ID 1565268, 9 pages
https://doi.org/10.1155/2022/1565268

Research Article

First-Principles Calculations to Investigate the Mechanical Structure and Optical Properties of Lead Halide Perovskite $CH_3NH_3PbI_3$

Truphena J. Kipkwarkwar, P. W. O. Nyawere, and C. M. Maghanga

Department of Biological and Physical Sciences, Kabarak University, P.O. Private Bag, Kabarak 20157, Kenya

Correspondence should be addressed to Truphena J. Kipkwarkwar; trukorir.09@gmail.com

Received 27 August 2021; Revised 26 December 2021; Accepted 12 January 2022; Published 16 February 2022

Academic Editor: Ram N. P. Choudhary

We report the study of the mechanical structure and optical properties of lead halide perovskite $CH_3NH_3PbI_3$ using *ab initio* methods. The ground state energy calculations were performed within density functional theory and generalized gradient approximation using the pseudopotential method with plane-wave basis sets. The norm conserving pseudopotential was used. The ground state properties of the electronic structure of the perovskite were used and elastic parameters such as bulk modulus B, Young's modulus E, shear modulus G, and Poisson's ratio υ were determined and found to be in good agreement with experimental values. The ratio B/G obtained was found to be greater than 1.75. Poisson's ratio (υ) was obtained as 0.25 implying that $CH_3NH_3PbI_3$ is a ductile material. The absorption coefficient within the energy range of 0 to 6 eV was found to be $5.76 \times 10^5\ cm^{-1}$ indicating maximum absorption. The absorption coefficient compares well with the available experimental and computed values.

1. Introduction

The desire to achieve high efficiency solar cells has led to research in perovskites that are lead-based, in particular lead halide perovskites. Since lead is not environmentally friendly, there has been a need to have organic lead halide perovskites with less lead, but organic lead-free perovskites are less stable [1]. Saliba et al. [2] reported that lead halide perovskites have become popular as photovoltaic materials due to their high power conversion efficiency (PCE) which stands at over 22%. The optical properties of these new materials are important not only to device design but also because of the insight they provide into less accessible properties such as energy band structures and binding energies, among other properties.

A study by Feng (2014), investigated the mechanical properties of hybrid organic-inorganic $CH_3NH_3BX_3$ (X = Br, I; B = Sn, Pb) perovskites used in photovoltaic cell absorbers. The structure consists of a network of corner-sharing BX_6 octahedra, where the B atom is a metal cation (Sn^{2+} or Pb^{2+}) and X is the hybrid anion (Br-, Cl^- or I^-). The dependent octahedra give room for a broad readjustment of the B-X-B bond angle, for this case, Pb-I-Pb. The various sets of joint rotations are called tilt transitions [3]. This develops symmetry, which shows different structures at varied temperatures. For instance, the three structural phases in which the compound $CH_3NH_3PbI_3$ exists include pseudocubic at increasing temperatures (above 327 K), tetragonal at room temperature, and orthorhombic at reducing temperatures (below 162.2 K) [3].

According to Zhu et al. 2021, the tetragonal phase changes to a cubic phase at 0.3 GPa. In addition to the 2H-phase, Young's modulus (E) reduces as pressure increases. This implies that the stiffness reduces with increasing pressure. Nonetheless, in orthorhombic, tetragonal, and cubic phases, as the pressure increases, E first increases and then reduces. In particular, the cubic phase has only three independent elastic constants: C_{11}, C_{12}, and C_{44} which were determined in this work [3, 4].

The crystal structures, elastic, and anisotropy properties of the $CH_3NH_3PbI_3$ were studied using the *ab initio* calculations.

The rationale of employing first-principles (*ab initio*) calculations was premised on the assertion that the mechanical properties of the compounds are relatively difficult to measure through an experimental approach. It was revealed that the absorption performance of perovskite solar cells greatly depends on the crystalline and stress state of the perovskite layer. The study by Bretschneider et al. [5] concurred with previously conducted work, and it indicated that the mechanical properties of perovskite are crucial for practical applications.

The study conducted by Sun et al. [6] analyzed factors that influence the mechanical properties of formamidinium lead halides and associated perovskites. The study formulated a systematic way of probing the mechanical properties of hybrid perovskite single crystals under nanoindentation. It was revealed that the shape, size, and hydrogen bonding resulting from the organic cations have a significant influence on their mechanical properties. Similarly, it was found that bonding in the inorganic framework and hydrogen bonding play a vital role in determining elastic stiffness.

The perovskite structure with the formula ABX_3 is used in many oxide compounds. In this study, A represents an organic positively charged ion ($CH_3NH_3^+$), *X* represents n halide specifically Iodide (I^-), and B is a divalent metal ion, in this case Pb^{2+}. This structure is a cubic unit cell which contains an A atom ($CH_3NH_3^+$) in the center of the cube, B atoms Pb^{2+} at the corners, and *X* atoms (I^-) at the center of the cell edges. The modelled pseudocubic structure is shown in Figure 1.

The calculated elastic parameters in this work include C_{11}, C_{12}, C_{44}, bulk modulus *B*, Young's modulus *E*, shear modulus *G*, Poisson's ratio *υ*, and anisotropy which describe the mechanical stability and ductility of $CH_3NH_3PbI_3$ [7, 8]. The study also noted that the measured Young's moduli (9.7–12.3 GPa) and hardness (0.36–0.45 GPa) reflected good mechanical flexibility and ductility. The study indicated that the mechanical properties of lead halide and related perovskites are important in device fabrication and performance.

The objective of this work is to establish the ideal mechanical and optical properties for photovoltaic applications from the first principle method. The rest of this paper is organized such that Section 2 is computational details, Section 3 is the results and discussions, and Section 4 deals with conclusions.

2. Computational Details

In this work, scalar relativistic electronic-structure calculations on this material were carried out based on density-functional theory (DFT) [9], plane waves, and the pseudopotential approach as implemented in the Quantum Espresso computer code [10]. In the calculation of total energy, the exchange-correlation potential is treated with the generalized gradient approximation of Perdew–Burke–Ernzerhof (GGA). The lattice constant of $CH_3NH_3PbI_3$ was well optimized [11, 12]. The total energy convergence in the iterative solution of the Kohn–Sham equations was fixed at 2×10^{-8} Rydberg (Ry), and self-consistency was achieved [13, 14]. All calculations were carried out under ground state conditions. The energy cut off was obtained as 30 Ry and $4\times4\times4$ k-point grid or more was found to be sufficient for this material.

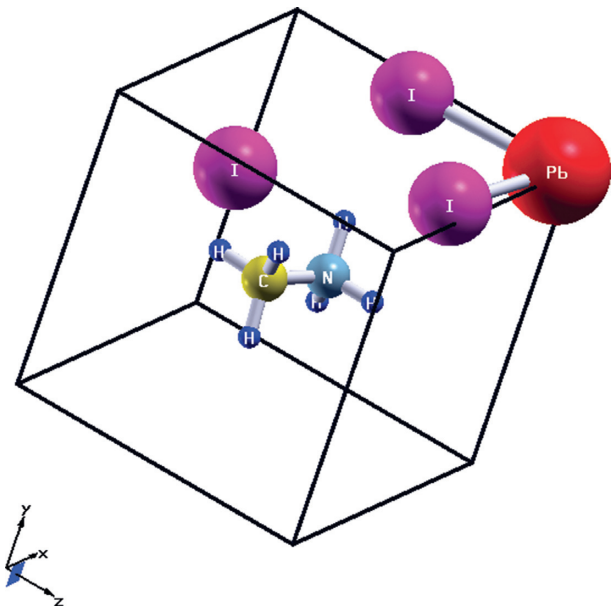

Figure 1: Crystal structure of $CH_3NH_3PbI_3$ of pseudocubic phase.

Core electrons were replaced by ab initio norm conserving pseudopotentials, generated using the Troullier–Martins scheme [15]. In the Kleinman–Bylander fully nonlocal separable representation [16]. According to this arrangement, s^1, $2s^22p$, $2s^22p^3$, $5s^25p^5$, and $5d^{10}6s^26p^2$ were used as valence electrons for H, C, N, I, and Pb, respectively. The large overlap between the semicore and valence states makes it possible for the semicore 5d electrons of Pb to be treated as valence electrons and distinctly included in the simulations, as explained in [17]. In this study, the electronic density, Hartree, and exchange correlation potentials were calculated in a uniform real-space grid with an equivalent plane-wave cutoff of 55 Ry in the representation of charge density. To integrate the Brillouin zone, we employed a Monkhorst–Pack sampling [18] equivalent to $13\times13\times13$ in a twelve-atom $CH_3NH_3PbI_3$ unit cell [19]. The ground state energies were determined by running the files in Appendices A and B. The determination of e-cut energy, alat, k-points, and the pseudocubic structure are the preliminary calculations determined for the optical and mechanical properties of $CH_3NH_3PbI_3$.

The approximations used in the calculation include the following: the exchange correlation GGA and the Voigt–Reuss–Hill approximation in calculating bulk, shear, and Young's modulus. Other types of approximations are beyond the objective of this study.

3. Results and Discussions

3.1. Mechanical Properties of $CH_3NH_3PbI_3$. Mechanical properties of solids include elasticity, strength, abrasion, hardness, ductility, brittleness, malleability, and toughness.

The elastic constants give the relation between dynamic properties and mechanical properties with respect to forces existing in materials.

The elastic constants of $CH_3NH_3PbI_3$ determined in this work are given in Table 1.

Table 1 shows the mechanical properties calculation of $CH_3NH_3PbI_3$ using the Quantum Espresso code, and results were compared with other available data. The average of the Voigt–Reuss–Hill approximations was used in calculating bulk (B), shear (G), and Young's modulus (E).

The results show that our calculated elastic constants for $CH_3NH_3PbI_3$ compare well with other work. These results confirm that pseudocubic $CH_3NH_3PbI_3$ is stable mechanically because it fulfills the Born stability criteria of cubic crystals whereby $C_{44} > 0$, $C_{11} > C_{12}$, and $C_{11} + 2C_{12} > 0$ [20]. The ratio B/G obtained was found to be greater than 1.75 implying that $CH_3NH_3PbI_3$ is a ductile material. These results confirm the ductility property of the perovskite [14, 21–23].

The computed anisotropic ratio which was obtained as 0.6 indicated that cubic $CH_3NH_3PbI_3$ was elastically anisotropic because of substituting it in the equation $A = (2C_{44}/C_{11} + C_{12})$. The value of A was obtained to be smaller than one ($A < 1$).

Poisson's ratio obtained was 0.25 which when rounded off to one decimal place is closely equal to 0.3 [24] which confirms that $CH_3NH_3PbI_3$ is a ductile material.

Table 1: Computed elastic constants such as C_{11}, C_{12}, C_{44}, bulk modulus (B), shear modulus (G), B/G ratio, Young's modulus (E), Poisson's ratio (υ), and anisotropy factor (A).

Computed elastic constants	This work	Computational results, Feng and Ciao, 2014
C_{11}	26.87	27.1
C_{12}	8.6	11.1
C_{44}	10.57	9.2
B	15.8	16.4
E	20.6	22.2
G	7.6	8.7
(υ)	0.25	0.28
B/G	2.08	1.89
A	0.6	—

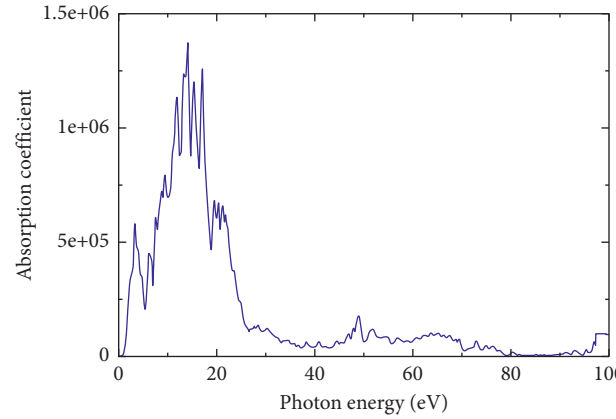

Figure 2: Absorption coefficient against photon energy.

3.2. Optical Properties of $CH_3NH_3PbI_3$. Optical properties of a material include reflectance, conductivity, absorption, refraction, transmittance, dispersion, diffraction, and so on. Solar panels, for example, need to absorb sufficient light energy. Therefore, a lower solar reflectance index rating is required of the material for high absorption. The solar transmittance of a surface is the fraction of the sun's radiation that is transmitted through the surface of the solar material. What is utilized by solar materials to produce electricity is the amount of solar radiation absorbed. This therefore prompted the study of absorption other than reflectance and transmittance as the main optical property in this work with respect to its suitability as a photovoltaic material. The absorption coefficient of $CH_3NH_3PbI_3$ has therefore been computed in this work.

The absorption coefficient shows how deep light rays will penetrate into a layer before it is absorbed. Light is rarely absorbed in a material with a low absorption coefficient. For a direct gap semiconductor like $CH_3NH_3PbI_3$, the absorption coefficient can reach elevated values.

A material that has a high optical absorption is suitable to be used in photovoltaic applications [25].

The high photovoltaic performance of $CH_3NH_3PbI_3$ is associated with optically high absorption characteristics. It is clear from Figure 2 that the material has a high absorption ability. Its absorption coefficient is about $1.4 \times 10^6\,\mathrm{cm}^{-1}$ for energy between 0 and 40 eV which contributes to the effective utilization of solar radiation.

This means that, with a high absorption coefficient, $CH_3NH_3PbI_3$ readily absorbs photons, which excite electrons from the valence band into the conduction band. In the solar spectrum, visible light is found within the range of wavelength $\lambda \approx 380$–780 nm which translates to energy of approximately 1.6–3.5 eV. Figure 3 indicates that at about 3.5 eV there is a peak in the absorption of the visible spectrum by $CH_3NH_3PbI_3$. The peak in Figure 3 gives the absorption coefficient within the given range of energy and it was found to be $5.76 \times 10^5\,\mathrm{cm}^{-1}$ indicating maximum absorption. This value can be compared with the derived absorption coefficient of $1.0978 \times 10^5\,\mathrm{cm}^{-1}$ [26] and $8.1448 \times 10^4\,\mathrm{cm}^{-1}$ [27] which greatly depends on the range at which the energy or wavelength was measured from. The data plotted in Figure 2 are in Appendix C.

The absorption coefficient determines how far into a material light of a particular wavelength or energy can pass through a material before it is absorbed. Absorption of solar energy will occur within the near UV region, visible region, and near infrared region between energy 0.886 eV and 3.98 eV. This is equivalent to a wavelength of 1400 nm–380 nm. This means that the material has a relatively wide absorption range, as shown by the wavelength. The high absorption coefficient of $CH_3NH_3PbI_3$ indicates that the material readily absorbs photons with energy equivalent to the band gap energy which excites electrons from the valence band into the conduction band.

The imaginary part of Figure 4 indicates a maximum absorption of photon energy between 0 and 5.0 eV, which is

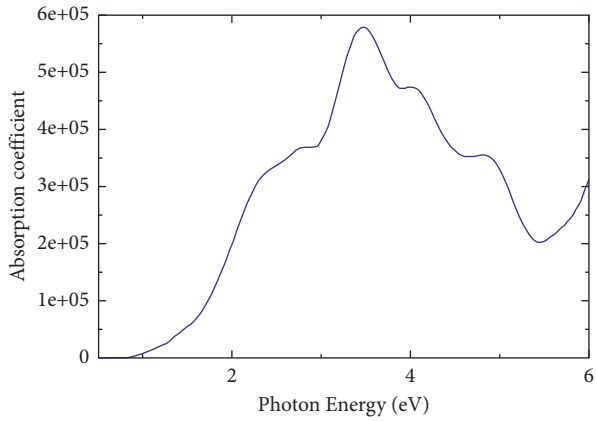

Figure 3: Absorption coefficient against photon energy (0–6 eV).

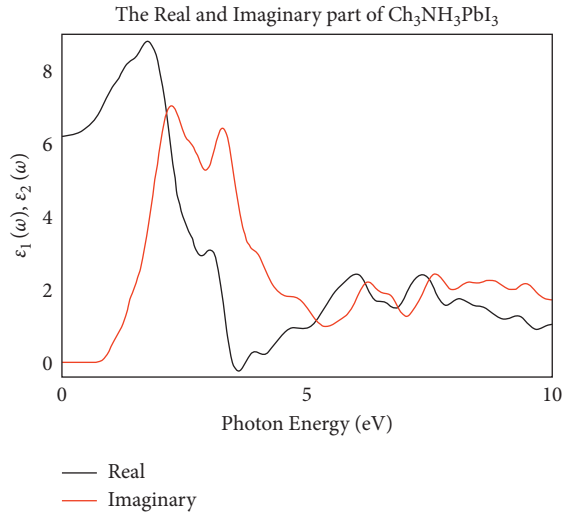

Figure 4: Real $\varepsilon_1(\omega)$ and imaginary $\varepsilon_2(\omega)$ part against the photon energy.

within the region where solar energy is utilized in a solar cell. $CH_3NH_3PbI_3$ has a band gap of 1.58 eV [28]. This means that only photons of energy equal to 1.58 eV will be absorbed by the material. Photons of higher or lower energy value than the band gap are wasted.

Figure 4 shows that the appearance of a sharp peak of the imaginary part of the dielectric constant of the $CH_3NH_3PbI_3$ implies the occurrence of strong absorption in this spectral region. The real part is related to the refractive index, while the imaginary part gives the absorption coefficient. The data plotted in the figure are in Appendix D.

Generally, a material with a high dielectric constant has a relatively less charge carrier recombination rate. As a result, the overall performance of optoelectronic devices is enhanced.

4. Conclusion

The result from the elastic constants done compares well with previously carried out work. The elastic parameters determined include bulk modulus B, Young's modulus E, shear modulus G, and Poisson's ratio v. The ratio B/G and Poisson's ratio obtained implied that $CH_3NH_3PbI_3$ is a ductile material. The evaluated elastic parameters enable us to conclude that the investigated compound is mechanically stable. This means that it can be molded into different shapes and sizes; therefore, suitable for the fabrication and modelling of solar cells.

Here, the optical constants which include absorption coefficients and real and imaginary components of the dielectric constant are reported. The value of the absorption coefficient within the spectral range of 0–6 eV within which the visible spectrum exists is $5.76 \times 10^5\,\mathrm{cm}^{-1}$. There was, however, inadequate literature from experimental and computational for the absorption coefficient to compare these results with, but from the results obtained, it can be concluded that $CH_3NH_3PbI_3$ has a high absorption coefficient of solar radiation and is highly suitable to be used in the fabrication and modelling of solar cells.

Appendix

A. Input file for pwscf code: Ecut.in, k-points.in and alat.in

```
&CONTROL
        title = "cubic_CH3NH3PbI3",
    calculation = "scf",
  restart_mode = "from_scratch",
    pseudo_dir = ". /",
    outdir = "./tmp",
        prefix = "pseudo",
        tstress = .true.,
    tprnfor = .true.,
/
&SYSTEM
        ibrav = 0,
        celldm(1) = 12.0772387957,
        nat = 12,
        ntyp = 5,
        nbnd = 50,
    ecutwfc = 40.0,
    ecutrho = 500.0,
  occupations = "smearing",
    smearing = "marzari-vanderbilt",
    degauss = 0.0075,
    !London_s6 = 0.750,
  ! London_rcut = 50.0,
  ! noncolin = .true.,
  ! lda_plus_u = .false.,
  ! lspinorb = .true.,
  ! nosym = .true.,
/
```

```
&ELECTRONS
        conv_thr = 1.0D-7,
/
ATOMIC_SPECIES
Pb 207.200Pb.pbe-mt_fhi.UPF
I 126.900 I.pbe-mt_fhi.UPF
H 1.008 H.pbe-mt_fhi.UPF
C 12.011C.pbe-mt_fhi.UPF
N 14.007N.pbe-mt_fhi.UPF
ATOMIC_POSITIONS {crystal}
C 0.3939882648252961 0.4998165502286085 0.4578307086810938
N 0.6090744378334350 0.5000072812331666 0.5477685929486071
H 0.4101503344735065 0.4996421926480608 0.2857772518934283
H 0.3086756133568471 0.6447043733807547 0.5110306384926346
H 0.3088856672784672 0.3549521469503247 0.5113014134206253
H 0.6962691547534092 0.6357485658144455 0.5015129819664779
H 0.6964106005070789 0.3642097749426654 0.5017817996551273
H 0.6063401459460280 0.5001870434389417 0.7112184893396645
Pb 0.9448835519577230 0.9999795897298682 0.9776228940296079
I 0.9094873486598019 0.9999820990246278 0.4751454839169895
I 0.8992708791277906 0.4999580210910821 0.0236644354684188
I 0.4323428768805755 0.9999948727175436 0.9224794036872126
K_POINTS {automatic}
13 13 13 0 0 0
```

B. Input file for pwscf code: Pseudo-Cubic structure

```
&CONTROL
title = "cubic_CH3NH3PbI3",
   calculation = "scf",
   restart_mode = "from_scratch",
      pseudo_dir = "./",
         outdir = "./tmp",
         prefix = "pseudo",
         tstress = .true.,
         tprnfor = .true.,
/
&SYSTEM
         ibrav = 0,
   celldm(1) = 12.0772387957,
         nat = 12,
         ntyp = 5,
         nbnd = 50,
      ecutwfc = 50.0,
      ecutrho = 500.0,
   occupations = "smearing",
      smearing = "marzari-vanderbilt",
         degauss = 0.0075,
      !London_s6 = 0.750,"
   ! London_rcut = 50.0,
   ! noncolin = .true.,
   ! lda_plus_u = .false.,
   ! lspinorb = .true.,
   ! nosym = .true.,
/
&ELECTRONS
        conv_thr = 1.0D-7,
/
ATOMIC_SPECIES
Pb 207.200Pb.pbe-mt_fhi.UPF
I 126.900 I.pbe-mt_fhi.UPF
H 1.008 H.pbe-mt_fhi.UPF
C 12.011C.pbe-mt_fhi.UPF
N 14.007N.pbe-mt_fhi.UPF
ATOMIC_POSITIONS {crystal}
C 0.3939882648252961 0.4998165502286085 0.4578307086810938
N 0.6090744378334350 0.5000072812331666 0.5477685929486071
H 0.4101503344735065 0.4996421926480608 0.2857772518934283
H 0.3086756133568471 0.6447043733807547 0.5110306384926346
H 0.3088856672784672 0.3549521469503247 0.5113014134206253
H 0.6962691547534092 0.6357485658144455 0.5015129819664779
H 0.6964106005070789 0.3642097749426654 0.5017817996551273
H 0.6063401459460280 0.5001870434389417 0.7112184893396645
Pb 0.9448835519577230 0.9999795897298682 0.9776228940296079
I 0.9094873486598019 0.9999820990246278 0.4751454839169895
```

I 0.8992708791277906 0.4999580210910821 0.0236644354684188
I 0.4323428768805755 0.9999948727175436 0.9224794036872126
K_POINTS {automatic}
13 13 13 0 0 0
CELL_PARAMETERS {alat}
1.0 0.0 0.0
0.0 1.0 0.0

C. Absorption coefficient. Out

0.0000000000000000 0.0000000000000000
1.9999978624805612E-002 0.24988928890946985
3.9999957249611223E-002 0.56433762654535935
5.9999935874416835E-002 0.93880409035995438
7.9999914499222446E-002 1.3637363347978548
9.9999893124028058E-002 1.8249222411118071
0.11999987174883367 2.3043054549207893
0.13999985037363930 2.7814219599502179
0.15999982899844489 3.2350568559897952
0.17999980762325052 3.6451955731050467
0.19999978624805612 3.9947583852990274
0.21999976487286174 4.2711463915435965
0.23999974349766734 4.4672020674000823
0.25999972212247296 4.5816254372279861
0.27999970074727859 4.6187371776105204
0.29999967937208416 4.5876703585826943
0.31999965799688979 4.5011851286911568
0.33999963662169541 4.3742003031563428
0.35999961524650104 4.2224078018739917
0.37999959387130661 4.0610222072591107
0.39999957249611223 3.9040452136353627
0.41999955112091786 3.7640632567371792
0.43999952974572348 3.6529455519580702
0.45999950837052905 3.5836006104679035
0.47999948699533468 3.5733897799420808
0.49999946562014030 3.6499273957827034
0.51999944424494593 3.8606612348911162
0.53999942286975156 4.2882586975166621
0.55999940149455718 5.0747471444112238
0.57999938011936270 6.4585256370478810
0.59999935874416832 8.8291054474426058
0.61999933736897395 12.805996207568926
0.63999931599377957 19.346607905096381
0.65999929461858520 29.890970541086375
0.67999927324339082 46.538939588370894
0.69999925186819645 72.272255963276436
0.71999923049300207 111.17399161491070
0.73999920911780759 168.70657806092615
0.75999918774261321 251.82732574133144
0.77999916636741884 369.29721031168708
0.79999914499222446 531.28329214132305
0.81999912361703009 749.89184290299875
0.83999910224183572 1037.2955829484670
0.85999908086664134 1407.5441140056985
0.87999905949144697 1871.1235629043078

D. Epsilon_imaginary data

0.0000000000000000 5.3344163605233434E-004
1.9999978624805612E-002 6.1341647492641534E-004
3.9999957249611223E-002 6.9270033738413005E-004
5.9999935874416835E-002 7.6831501735604530E-004
7.9999914499222446E-002 8.3720472518939446E-004
9.9999893124028058E-002 8.9646173515729776E-004
0.11999987174883367 9.4355558235892508E-004
0.13999985037363930 9.7654034997798542E-004
0.15999982899844489 9.9421597189845528E-004
0.17999980762325052 9.9622441246949539E-004
0.19999978624805612 9.8306940473013942E-004
0.21999976487286174 9.5605795049326185E-004
0.23999974349766734 9.1717153941446345E-004
0.25999972212247296 8.6888354097770174E-004
0.27999970074727859 8.1394522609164774E-004
0.29999967937208416 7.5516561144114915E-004
0.31999965799688979 6.9520960676005248E-004
0.33999963662169541 6.3643521379392102E-004
0.35999961524650104 5.8078475824888121E-004
0.37999959387130661 5.2973874225868385E-004
0.39999957249611223 4.8433556982319375E-004
0.41999955112091786 4.4525793070104391E-004
0.43999952974572348 4.1298883291785365E-004
0.45999950837052905 3.8804883906635231E-004
0.47999948699533468 3.7134244973854934E-004
0.49999946562014030 3.6466686038921385E-004
0.51999944424494593 3.7147087673180520E-004
0.53999942286975156 3.9799477086350474E-004
0.55999940149455718 4.5497040612939641E-004
0.57999938011936270 5.6010896872353295E-004
0.59999935874416832 7.4164052921932842E-004
0.61999933736897395 1.0431792142133784E-003
0.63999931599377957 1.5301479011784957E-003
0.65999929461858520 2.2978804873596687E-003
0.67999927324339082 3.4813009216057358E-003
0.69999925186819645 5.2657362272757581E-003

0.71999923049300207 7.8979530811855176E-003
0.73999920911780759 1.1695941614998524E-002
0.75999918774261321 1.7055375221479332E-002
0.77999916636741884 2.4450168760568370E-002
0.79999914499222446 3.4424301272587242E-002
0.81999912361703009 4.7572249380705797E-002
0.83999910224183572 6.4506167837405079E-002
0.85999908086664134 8.5809463239980802E-002
0.87999905949144697 0.11197862125151939
0.89999903811625248 0.14335787776702530
0.91999901674105811 0.18007418318359733
0.93999899536586373 0.22198233191398303
0.95999897399066936 0.26863145189750798
0.97999895261547498 0.31926363677986730
0.99999893124028061 0.37285291769071954
1.0199989098650861 0.42818793275882622
1.0399988884898919 0.48399495898381956
1.0599988671146974 0.53909032711788785
1.0799988457395031 0.59254396568353462
1.0999988243643086 0.64383043953689467
1.1199988029891144 0.69294178874874912
1.1399987816139199 0.74043873248399739
1.1599987602387254 0.78742366009403986
1.1799987388635311 0.83542968261332895
1.1999987174883366 0.88623337705947192
1.2199986961131424 0.94161255363725804
1.2399986747379479 1.0030819184598672
1.2599986533627536 1.0716465364865613
1.2799986319875591 1.1476137801871984
1.2999986106123647 1.2304982469674299
1.3199985892371704 1.3190414491487927
1.3399985678619759 1.4113506783977086
1.3599985464867816 1.5051420937798612
1.3799985251115872 1.5980551241329874
1.3999985037363929 1.6879920359219860
1.4199984823611984 1.7734306594810392
1.4399984609860041 1.8536612208947241
1.4599984396108097 1.9289098225606267
1.4799984182356152 2.0003295041545823
1.4999983968604209 2.0698617419319114
1.5199983754852264 2.1399926391000825
1.5399983541100322 2.2134448548321810
1.5599983327348377 2.2928553128071814
1.5799983113596434 2.3804883060552258
1.5999982899844489 2.4780241295852918
1.6199982686092544 2.5864470927814649
1.6399982472340602 2.7060373502894897
1.6599982258588657 2.8364526354191395
1.6799982044836714 2.9768724128578605
1.6999981831084769 3.1261705799078925
1.7199981617332827 3.2830841733208844
1.7399981403580882 3.4463532349661103
1.7599981189828939 3.6148182943263047
1.7799980976076994 3.7874734974121771
1.7999980762325050 3.9634822767638465
1.8199980548573107 4.1421668071491693
1.8399980334821162 4.3229820983417309
1.8599980121069219 4.5054817171988359
1.8799979907317275 4.6892770608661660
1.8999979693565332 4.8739882487202300
1.9199979479813387 5.0591838385795160
1.9399979266061442 5.2443092428345723
1.9599979052309500 5.4286090618276290
1.9799978838557555 5.6110546037395288
1.9999978624805612 5.7902922230998595
2.0199978411053667 5.9646287562902094
2.0399978197301722 6.1320663036618575
2.0599977983549782 6.2903903787222353
2.0799977769797837 6.4373048392859573
2.0999977556045892 6.5705967031423533
2.1199977342293947 6.6883066792904744
2.1399977128542003 6.7888790441831928

Epsilon_real data

0.0000000000000000 6.1931430714863174
1.9999978624805612E-002 6.1930407053608993
3.9999957249611223E-002 6.1938563165439566
5.9999935874416835E-002 6.1952602650718536
7.9999914499222446E-002 6.1974188783175936
9.9999893124028058E-002 6.2001635124067249
0.11999987174883367 6.2036276978490914
0.13999985037363930 6.2077047955494074
0.15999982899844489 6.2124936700755589
0.17999980762325052 6.2179332914075323
0.19999978624805612 6.2240873135519514
0.21999976487286174 6.2309352781792882
0.23999974349766734 6.2385086582781115
0.25999972212247296 6.2468205793321721
0.27999970074727859 6.2558780504138731
0.29999967937208416 6.2657182831588996
0.31999965799688979 6.2763347127658138
0.33999963662169541 6.2877787977445880
0.35999961524650104 6.3000418337295070
0.37999959387130661 6.3131817397213261
0.39999957249611223 6.3271974203390187

0.41999955112091786 6.3421488942209638
0.43999952974572348 6.3580500157800977
0.45999950837052905 6.3749618213386903
0.47999948699533468 6.3929194278858397
0.49999946562014030 6.4119851363227189
0.51999944424494593 6.4322246799813900
0.53999942286975156 6.4536981757555782
0.55999940149455718 6.4765228860092847
0.57999938011936270 6.5007374161166362
0.59999935874416832 6.5265604918032594
0.61999933736897395 6.5539458718415728
0.63999931599377957 6.5833275146239361
0.65999929461858520 6.6144091802505738
0.67999927324339082 6.6480812360975916
0.69999925186819645 6.6834291680622213
0.71999923049300207 6.7222692359673326
0.73999920911780759 6.7623527816891649
0.75999918774261321 6.8072501683346873
0.77999916636741884 6.8521655927265339
0.79999914499222446 6.9037265999087314
0.81999912361703009 6.9528217471509564
0.83999910224183572 7.0109225112799392
0.85999908086664134 7.0624530633516347
0.87999905949144697 7.1257763832343066
0.89999903811625248 7.1768458619097073
0.91999901674105811 7.2426868033388434
0.93999899536586373 7.2897416623388365
0.95999897399066936 7.3544137898459638
0.97999895261547498 7.3943723762011837
0.99999893124028061 7.4543559473016163
1.0199989098650861 7.4860425618861326
1.0399988884898919 7.5395705027294309
1.0599988671146974 7.5647061849061190
1.0799988457395031 7.6129967079255350
1.0999988243643086 7.6359197626346651
1.1199988029891144 7.6831248519037869
1.1399987816139199 7.7089289719086684
1.1599987602387254 7.7603687375998396
1.1799987388635311 7.7921164700806198
1.1999987174883366 7.8513903994426562
1.2199986961131424 7.8879042658708629
1.2399986747379479 7.9544121471852272
1.2599986533627536 7.9901775467922800
1.2799986319875591 8.0587087460349913
1.2999986106123647 8.0863856040828548
1.3199985892371704 8.1494352580231979
1.3399985678619759 8.1638648741230089
1.3599985464867816 8.2156774821848337
1.3799985251115872 8.2171195748464037
1.3999985037363929 8.2571961419267534
1.4199984823611984 8.2517276554436947
1.4399984609860041 8.2856108846676442
1.4599984396108097 8.2822147326230358
1.4799984182356152 8.3189045250075750
1.4999983968604209 8.3248173993501524
1.5199983754852264 8.3722381800163710
1.5399983541100322 8.3892290017448623
1.5599983327348377 8.4503657869141549
1.5799983113596434 8.4739747286059028
1.5999982899844489 8.5457616481593366
1.6199982686092544 8.5675891034743401
1.6399982472340602 8.6427744165441478
1.6599982258588657 8.6540838504358391
1.6799982044836714 8.7244979680524750
1.6999981831084769 8.7189580821958401
1.7199981617332827 8.7781349652435487
1.7399981403580882 8.7525824212454921
1.7599981189828939 8.7966422972368576
1.7799980976076994 8.7502384111226039
1.7999980762325050 8.7773121872047675
1.8199980548573107 8.7102000926946239
1.8399980334821162 8.7193366048877454
1.8599980121069219 8.6316005820129824
1.8799979907317275 8.6218215288485034
1.8999979693565332 8.5129052407281112
1.9199979479813387 8.4825424518298718
1.9399979266061442 8.3510676740884833
1.9599979052309500 8.2974210369209054
1.9799978838557555 8.1415736368657541
1.9999978624805612 8.0611925032699929
2.0199978411053667 7.8798923233898259
2.0399978197301722 7.7697790521169425
2.0599977983549782 7.5643487630065671
2.0799977769797837 7.4237936848135018
2.0999977556045892 7.1991957759046308
2.1199977342293947 7.0312540631126010
2.1399977128542003 6.7959420381638100

Data Availability

The density functional theory (DFT) codes were used in this work to run the input files to obtain the output data used in this work. The code used is available at https://www.quantum-espresso.org/. Pseudopotentials and other resources on the study material are available on the website. The other data supporting this research work are from previously reported

studies and datasets, which have been cited. Some of the input files used to process data have been given in the appendices of the document.

Conflicts of Interest

The authors declare that they have no conflicts of interest.

Acknowledgments

The authors gratefully acknowledge the computer resources, technical expertise, and assistance provided by the Centre for High-Performance Computing (CHPC), Cape Town, South Africa.

References

[1] V. K. Prashant, B. Juan, and B. Jilian, "Lead-free perovskite solar cells," *ACS Energy Letters*, vol. 2, pp. 904-905, 2017.

[2] M. Saliba, T. Matsui, J.-Y. Seo et al., "Cesium-containing triple cation perovskite solar cells: improved stability, reproducibility and high efficiency," *Energy & Environmental Science*, vol. 9, no. 6, pp. 1989–1997, 2016.

[3] J. Feng, "Mechanical properties of hybrid organic-inorganic CH3NH3BX3 (B = Sn, Pb; X = Br, I) perovskites for solar cell absorbers," *APL Materials*, vol. 2, no. 8, Article ID 081801, 2014.

[4] H. Zhu, H. Chen, H. Zhu et al., "First-principles calculations of the structural and elastic properties of CH3NH3PbI3 under high pressure," *Brazilian Journal of Physics*, vol. 52, no. 1, p. 18, 2022.

[5] S. A. Bretschneider, J. Weickert, J. A. Dorman, and L. Schmidt-Mende, "Research Update: physical and electrical characteristics of lead halide perovskites for solar cell applications," *APL Materials*, vol. 2, no. 4, Article ID 040701, 2014.

[6] S. Sun, F. H. Isikgor, Z. Deng et al., "Factors influencing the mechanical properties of formamidinium lead halides and related hybrid perovskites," *ChemSusChem*, vol. 10, no. 19, pp. 3740–3745, 2017.

[7] K. Bidai, M. Ameri, S. Amel et al., "First-principles calculations of pressure and temperature dependence of thermodynamic properties of anti-perovskite BiNBa 3 compound," *Chinese Journal of Physics*, vol. 55, no. 5, pp. 2144–2155, 2017.

[8] S. Das, M. Debbarma, D. Ghosh et al., "First-principles calculations to investigate structural, mechanical, electronic, magnetic and thermoelectric properties of Ba2CaMO6 (M= Re, Os) cubic double perovskites," *Physica B: Condensed Matter*, vol. 626, Article ID 413554, 2021.

[9] P. Hohenberg and W. Kohn, "Inhomogeneous electron gas," *Physical Review*, vol. 136, no. 3B, pp. B864–B871, 1964.

[10] P. Giannozzi, S. Baroni, N. Bonini et al., "Quantum ESPRESSO: a modular and open-source software project for quantum simulations of materials," *Journal of Physics: Condensed Matter*, vol. 21, no. 39, Article ID 395502, 2009.

[11] J. P. Perdew, K. Burke, and M. Ernzerhof, "Generalized gradient approximation made simple," *Physical Review Letters*, vol. 77, no. 18, pp. 3865–3868, 1996.

[12] A. Ilyas, S. A. Khan, K. Liaqat, and T. Usman, "Investigation of the structural, electronic, magnetic, and optical properties of CsXO3 (X = Ge, Sn, Pb) perovskites: a first-principles calculations," *Optik*, vol. 244, Article ID 167536, 2021.

[13] W. Kohn and L. J. Sham, "Self-consistent equations including exchange and correlation effects," *Physical Review*, vol. 140, no. 4A, pp. A1133–A1138, 1965.

[14] R. Arar, T. Ouahrani, D. Varshney et al., "Structural, mechanical and electronic properties of sodium based fluoroperovskites NaXF3 (X=Mg, Zn) from first-principle calculations," *Materials Science in Semiconductor Processing*, vol. 33, pp. 127–135, 2015.

[15] N. Troullier and J. L. Martins, "Efficient pseudopotentials for plane-wave calculations," *Physical Review B*, vol. 43, no. 3, pp. 1993–2006, 1991.

[16] L. Kleinman and D. M. Bylander, "Efficacious form for model Pseudopotentials," *Physical Review Letters*, vol. 48, no. 20, pp. 1425–1428, 1982.

[17] J. Sifuna, P. García-Fernández, G. S. Manyali, G. Amolo, and J. Junquera, "First-principles study of two-dimensional electron and hole gases at the head-to-head and tail-to-tail 180° domain walls in PbTiO3 ferroelectric thin films," *Physical Review B*, vol. 101, no. 17, Article ID 174114, 2020.

[18] H. J. Monkhorst and J. D. Pack, "Special points for brillouin-zone integrations," *Physical Review B*, vol. 13, no. 12, pp. 5188–5192, 1976.

[19] R. Dalven, *Empirical~& Relation between Energy Gap and Lattice Constant in Cubic Semiconductors*, University of California, Berkeley, CF, USA, 1973.

[20] H. Fu, D. Li, F. Peng, T. Gao, and X. Cheng, "Ab initio calculations of elastic Constants and thermodynamic properties of NiAl under high Pressures," *Computational Materials Science*, vol. 44, no. 2, pp. 774–778, 2008.

[21] F. Litimein, R. Khenata, A. Bouhemadou, Y. Al-Douri, and S. B. Omran, "First-principle calculations to investigate the elastic and thermodynamic properties ofRBRh3(R = Sc, Y and La) perovskite compounds," *Molecular Physics*, vol. 110, no. 2, pp. 121–128, 2012.

[22] F. Mouhat and F.-X. Coudert, "Necessary and sufficient elastic stability conditions in various crystal systems," *Physical Review B*, vol. 90, no. 22, Article ID 224104, 2014.

[23] N. Moulay, M. Ameri, Y. Azaz, A. Zenati, Y. Al-Douri, and I. Ameri, "Predictive study of structural, electronic, magnetic and thermodynamic properties of XFeO3 (X = Ag, Zr and Ru) multiferroic materials in cubic perovskite structure: first-principles calculations," *Materials Science-Poland*, vol. 33, no. 2, pp. 402–413, 2015.

[24] S. F. Pugh, "XCII. Relations between the elastic moduli and the plastic properties of polycrystalline pure metals," *The London, Edinburgh, and Dublin Philosophical Magazine and Journal of Science*, vol. 45, no. 367, pp. 823–843, 1954.

[25] J. U. Rehman, M. Usman, M. B. Tahir et al., "First-principles calculations to investigate ultra-wide bandgap semiconductor behavior of NaMgF3 fluoro-perovskite with external static isotropic pressure and its impact on optical properties," *Optik*, vol. 23, Article ID 168532, 2021.

[26] J. M. Ball, S. D. Stranks, M. T. Hörantner et al., "Optical properties and limiting photocurrent of thin-film perovskite solar cells," *Energy & Environmental Science*, vol. 8, no. 2, pp. 602–609, 2015.

[27] L. J. Phillips, A. M. Rahed, R. E. Treharne et al., "Maximizing the optical Performance of planar CH3NH3PbI3 hybrid perovskite heterojunction stacks," *Solar Energy Materials and Solar Cells*, vol. 147, pp. 37–333, 2016.

[28] T. J. Kipkwarkwar, P. Nyawere, and C. Maghanga, "Ab initio study of electronic, mechanical and optical properties of CH3NH3PBI3 for photovoltaic application," Thesis, Kabarak University, Nakuru, Kenya, 2021.